Pulsation Velocity Curves for 3 Cepheid Variables

Kevin B. Stevenson*

Department of Astronomy, University of Western Ontario, London, ON, N6A 3K7, Canada

ABSTRACT

A total of 44 usable observations were made of three of the brightest Classical Cepheids in the sky, δ Cephei, η Aquilae and ζ Geminorum. In each exposure, four Fe I spectral lines in the 6250 Å region were normalized, converted to a velocity span, averaged, then fitted by a model. The resulting model parameters from each exposure were then used to create a pulsation velocity curve as a function of phase and without the use of a projection factor typically used in other techniques. Acceptable agreement is found in comparing the radial velocity curves with Barnes, Bersier and Nardetto. The amplitudes of radius variation, used in the Baade-Wesselink method, were determined to be 3.54×10^6, 4.59×10^6 and 4.75×10^6 km for δ Cephei, η Aquilae and ζ Geminorum, respectively.

Keywords: Cepheid variables, Delta Cephei, Eta Aquilae, Zeta Geminorum, radial velocity, Baade-Wesselink

1. INTRODUCTION

A Cepheid variable is a particular type of variable star, an intrinsic pulsating variable. The variability is caused by physical changes within the star itself which causes its radius to expand and contract periodically. This process is part of its natural evolution as it ages and occurs in the instability strip of the Hertzsprung-Russell (HR) Diagram. A Cepheid varies in luminosity and spectral type with a generally stable, well determined period. Once its period is known, the star's absolute magnitude can be precisely determined using the following empirically derived relation:

$$M_\nu = -2.76\, log(\Pi) - 1.4, \tag{1}$$

where M_ν is the absolute magnitude and Π is the period in days. This implies that a longer period of pulsation results from a more luminous star. This relation allows a Cepheid variable to act as standard candle when trying to determine the distance to its host cluster or galaxy. Note that there is also a minor dependence on metallicity that is not used in the equation above.

The Baade-Wesselink method is used to calculate the stellar radii of certain pulsating stars, including Cepheid variables. To accomplish this, two different types of measurements must be made. First, the star's flux (F) and surface brightness (σ) must be determined at two different points in its period, say at maximum and minimum radius. The ratio of these radii can then be determined by the following relation:

$$\frac{R_{max}}{R_{min}} = \sqrt{\frac{F(R_{max})/\sigma(R_{max})}{F(R_{min})/\sigma(R_{min})}}. \tag{2}$$

Second, the spectra of a variable star must be observed, with good phase coverage over its pulsation period, in order to produce a pulsation velocity curve. This curve indicates the velocity at which the star is expanding or contracting at any point in its phase. Knowing this, the difference between the two radii chosen above ($R_{max} - R_{min}$ in our case) can be calculated by summing up the products of velocity and time between two consecutive time intervals. The result is two equations with two unknowns thus making it easy to solve for the two radii. One can also device a distance, d, in parsecs (pc) to the pulsating variable by substituting the above results into this equation:

$$d = 9.305\frac{R}{\theta} = 9.305\frac{R_{max} - R_{min}}{\Delta\theta} \tag{3}$$

where $\theta = \sqrt{\frac{F}{\pi\sigma}}$ is the mean angular diameter in miliarcseconds (mas) and R is in units of solar radii. The mean angular diameter, and sometimes the angular diameters variations, $\Delta\theta$, can be accurately measured using

*Corresponding author: ksteve24@uwo.ca

long-baseline interferometry.[1] Keep in mind, however, that all of these variables are wavelength dependent and for consistency, both sets of measurements should be accomplished at similar wavelengths.

In order for a star to be pulsationally unstable, the driving regions within the star must overpower the effects of the damping regions. This assertion is based on linear theory but so far also applies to nonlinear pulsations and hence can be applied presumably to real stars as well. There are two main types of destabilization mechanisms: nuclear driving and envelope ionization mechanisms. The former results from thermodynamic nuclear reactions near the stellar center and is considered to be a negligible source for pulsations in a classical Cepheid. The latter involves the modulation of the flux through the stellar envelope and is heavily favored as being the principle source of pulsation. Cox[2] has shown that flux modulations have the proper phasing to drive the pulsations and under the right circumstances can even induce pulsational instability in a star. By his calculations, the source of $80-90\%$ of the driving is the once ionized helium ionization zone, where it is in the midstages of ionizing to second helium ionization ($He^{+} \rightleftharpoons He^{2+}$), while the remainder occurs in the hydrogen ionization zone ($H \rightleftharpoons H^{+}$). These zones exist in the envelope of the pulsating star and at certain phases the hydrogen ionization front (HIF) may even interact with the photosphere itself.

Variation in the brightness of a Cepheid is mostly due to temperature variations, while changes in radius have only a minor effect ($\leq 10\%$). The maximum brightness occurs when the Cepheid is at its earliest spectra (usually F type) while the minimum brightness occurs at the latest spectra (G type). This, however, does not coincide with its minimum and maximum radius. There is a phase lag discrepancy that causes a retardation of maximum brightness behind minimum radius on the order of $0.1-0.2$ periods. The maximum brightness usually occurs close to when the star is expanding through its equilibrium radius, which corresponds to a minimum (most negative) radial velocity. This is based on the convention that the radial velocity is negative when the star is expanding towards the observer and positive when it is contracting away from the observer.

The radial velocity is the velocity of an object along the observer's line of sight. Emitted light from a receding star experiences a Doppler shift that increases it's wavelength thus making it appear redder (redshifted). Similarly, the wavelength of the light from a rapidly approaching star will decrease thus causing the object to appear more blue (blueshifted). The average Cepheid is moving at about 25 km/s relative to our solar system therefore tends to have a substantial systemic radial velocity (v_γ). The radial velocity of a star can be determined by looking at its spectrum and comparing the star's measured wavelength of a narrow spectral line with the true wavelength as measured in a laboratory. This change in wavelength can be converted into a corresponding velocity shift using the following relation:

$$\frac{\Delta\lambda}{\lambda} = \frac{\Delta v}{c}, \tag{4}$$

where λ is the wavelength, v is the velocity, and c is the speed of light in a vacuum. The radial velocity of most stars is considered to be constant, once the barycenter corrections have been made, however the pulsations of a Cepheid variable are large enough to cause a significant oscillation in its overall radial velocity. Thus a barycenter corrected Cepheid variable has two radial velocity components: the systemic component (v_γ) due to its heliocentric motion and the pulsation component (V_{puls}) due to its instability.

The weak spectral lines of a Cepheid variable are quite broad and tend to be asymmetric, thus making it difficult to assign a specific wavelength to a spectral line. As a result, several methods have been developed to measure radial velocities. These include the line minimum method, generally determined by fitting a parabola to several pixels about the local minima, the Gaussian fit method, which uses a symmetric Gaussian profile, the line bisector method, where the width of the line is measured at various depths, and the line centroid method, determined by integrating the line profile.[3] As a result of foreshortening and limb darkening, all of these methods require a projection factor, $p \approx 1.40$, which is multiplied with the systemically corrected observed radial velocity ($V_{rad} - v_\gamma$) to determine the actual radial velocity, hereafter referred to as the pulsation velocity, V_{puls}.

$$V_{puls} = p\,(V_{rad} - v_\gamma) \tag{5}$$

Nardetto at al.[3] suggest using line centroid based methods for radial velocities of Cepheid variables because the centroid projection factor is independent of the width of the spectral line and the rotation velocity. The projection factors of the other methods are not independent of these variables and as such may vary significantly throughout a Cepheid's pulsation period.

Star	δ Cep	η Aql	ζ Gem
RA[5] (J2006.5)	22h 29m 24.8s	19h 52m 48.2s	7h 4m 29.6s
Dec[5] (J2006.5)	+58° 26' 55"	+1° 1' 22'	+20° 33' 37"
Period[4, 6] (Days)	5.366341	7.176775	10.14901
Spectral Range[6]	F5Ib - G1Ib	F6Ib - G4Ib	F7Ib - G3Ib
Apparent Magnitude[6]	3.48 - 4.37	3.48 - 4.39	3.62 - 4.18
Ephemeris[6] (+2450000)	1809.556812	1808.676431	1814.85297

Table 1. Parameters for the observed Cepheid variables

This paper will investigate pulsation velocity curves for classical Cepheids by combining observations and models to reproduce the curves without the use of a projection factor. The goal is to produce reliable amplitudes of radius variation to be used in the Baade-Wesselink method. Three classical Cepheids have been chosen for observation: δ Cephei, η Aquilae and ζ Geminorum. These stars were chosen specifically because they are visible from our location in the northern hemisphere and they are adequately bright for our telescope and exposure limits. Their parameters are given in Table 1. The ephemeris specifies the Julian Date of maximum intensity for each star and is used as the period's zero point, as is convention. The period for δ Cephei was taken from the Combined General Catalogue of Variable Stars (Vol. I-III) while η Aquilae and ζ Geminorum's periods were calculated using the following formulae provided by Szabados.[4]

η Aquilae:

$$C = 2442794.726 + 7.176726\,E \tag{6}$$

$$\Pi = 7.176726 + 3.16 \times 10^{-8}\,E \tag{7}$$

ζ Geminorum:

$$C = 2443785.438 + 10.150074\,E \tag{8}$$

$$\Pi = 10.150074 - 10.76 \times 10^{-7}\,E \tag{9}$$

The chosen date, C, is used to solve for E, the number of periods between the two Julian Dates, which then can be used to determine the period, Π. The mean Julian Date for each star's set of exposures was used for C, namely 2453871.357 for η Aquilae and 2453801.959 for ζ Geminorum. Though ζ Geminorum's period is decreasing quite rapidly, it can be considered to be constant over its six month observing season, with a change of less than 0.0002% or 0.00002 days.

The remainder of this paper is organized as follows: Section 2 describes the observatory, how the spectral observations were made and the software used to reduce and model the data, Section 3 covers the analysis of the data and delivers the corresponding results, and Section 4 makes some important conclusions based on these results. After the list of references is an appendix of model and observational data for the three Cepheids.

2. OBSERVATIONS AND REDUCTIONS

Spectroscopic observations are made at the Elginfield Observatory, near the University of Western Ontario, using a 1.2 m telescope, a 4096x200 pixel CCD detector and a spectrograph at the coudé focus. Measurements are centered on $\lambda = 6250$ Ångströms with a field of ≈ 65 Å. The resolving power is approximately 10^5 with signal-to-noise ratios of approximately 250 for this project.[7, 8] Observations were made by Kevin B. Stevenson (KBS), Dr. David F. Gray (DFG) and Kevin Brown (KB) between October of 2005 and August of 2006 as part of a Masters project under the supervision and helpful guidance of Dr. Gray.

A diagram of the coudé room, which houses the spectrograph, can be seen in Figure 1. The operation of this spectrograph is as follows. Light from the telescope passes through a 6250 Å filter located on the filter wheel and is focused onto the entrance slit, which uses a Richardson image slicer to recycle any lost light not falling directly on the slit back onto the slit. Next, a collimator mirror is placed at its focal length from the entrance slit to produce parallel light rays onto the diffraction grating. The light is then dispersed using a blazed grating

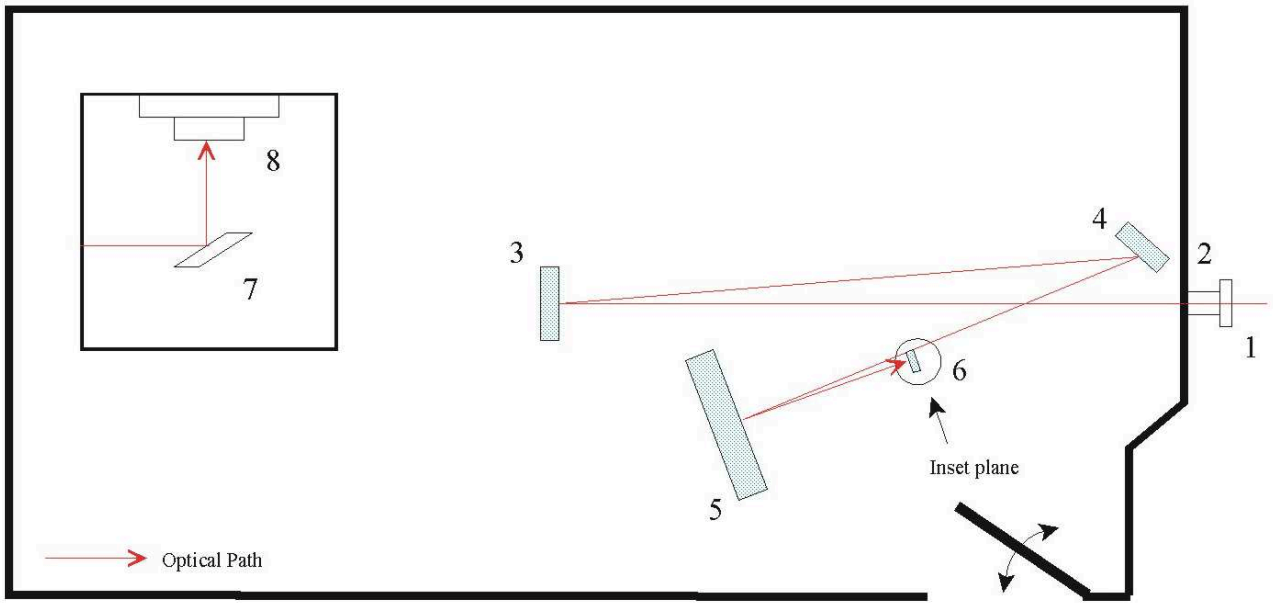

This overhead view shows:

1. The filter wheel
2. The image slicer
3. The collimator mirror
4. The diffraction grating
5. The camera mirror
6. Coude spectrograph detector assembly (see inset for side view)
7. The pick-off mirror
8. The CCD detector

Figure 1. A schematic of the Elginfield Observatory coudé spectrograph[9]

that can be rotated to select the desired wavelength. Finally, a camera mirror focuses the dispersed light, with the help of a pick-off mirror, onto a CCD detector located at the camera mirror's focal length.

All of the utility programs mentioned below are part of a custom software package written and provided by Dr. Gray. The raw data is reduced using the R9 program which requires a dark field, a bias field and a flat field to remove instrumental effects in the raw data from the CCD. Each of the 4096 columns is averaged over the 200 rows in bins of 10 to produce a final spectrum used in analysis. SPLT is used to normalize the full length of the continuum in each spectrum to a value of 1. A total of six lines were selected for further analysis: 6231, 6233, 6238, 6248, 6253 and 6265 Å. These Fe I and Fe II lines were chosen because they are weak, unblended and relatively insensitive to temperatures changes. The individual profiles are edited to remove spurious data points and adjacent spectral lines by choosing reasonable values close or equal to the continuum. A spectral line's asymmetry can be easily visualized using a line bisector, which consists of the midpoints of horizontal line segments extending across the profile.[10] The BISM software program generates one bisector point for each observed point on one side of the profile. Connecting the points results in the line bisector. Illustrations of line bisectors are available in the Section 3.

The DISPER program is used to obtain an absolute wavelength scale for a spectral line relative to each exposure. This is accomplished by analyzing the spectrum of two telluric lamps taken just prior to each star exposure and two lamps taken just following. The telluric lines act as a stable, uncompromised reference spectrum against which the Doppler shift of an astronomical body can be compared.[11] Because the spectrum on the CCD can shift from night to night, and even from exposure to exposure, the locations of the telluric lines must be accurately determined before and after each exposure. To complete the DISPER program, the barycenter correction must be taken into account. VSUN3 is used to compute the barycentric velocity using the input from PHASER, PHIN.SC, which contains the date, time and length of each exposure. The PHASER program utilizes PHIN.SC to phase the exposures according to a given period. In this case, the Cepheid variables' respective

periods, as given in Table 1, are used with PHASER to determine the phase coverage and for providing the appropriate offset when plotting certain graphs.

The disk integration program, DSKI4, is necessary for developing models that fit each phase of an observed spectral line. A series of model spectral lines is created by varying the following parameters: the projected rotation velocity ($V_{rot} \sin i$), the radial velocity (V_{rad}), the radial/tangential macroturbulence (ζ_{RT}), the limb darkening coefficient (u_V), and an isotropic factor that consists of macroturbulence, microturbulence and thermal components (ζ_{ISO}). The radial velocity has two contributions, the radial/tangential factor (V_{RT}) as well as the isotropic factor (V_{ISO}). Both are weighted according to the given model input parameters then added together to determine the true radial velocity. It is not necessary for the two radial velocity contributions to have the same velocity shift in the presence of a velocity gradient through the Cepheid's line-forming region.[12] The radial/tangential macroturbulence (ζ_{RT}) affects mostly the core of a spectral line whose depth of formation is much shallower than that of its wings, whose main contribution is the ζ_{ISO} factor. Because of the velocity gradient in the photosphere, the line's core will typically have a larger absolute radial velocity than its wings thus requiring a larger absolute V_{RT} as compared to V_{ISO}. In over 86% of our models, $|V_{RT}| \geq |V_{ISO}|$. The bulk of the remaining models occur in δ Cephei between the phases 0.95 and 0.35 and could be the result of a lag between the collapsing higher layers and the deeper layers being suddenly driven to expand.

In order to reduce, or sometimes merely restrict, the number of free parameters in our models, many of the variables are held constant for a particular star. These variables include the projected rotation velocity, the limb darkening coefficient and the ζ ratio of the radial velocities, all discussed below in further detail.

The projected rotation velocity ($V_{rot} \sin i$) must be used with great care in the models to achieve a proper fit. Even without the $V_{rot} \sin i$ component, the spectral lines are significantly broadened with the proper isotropic contributions, which incorporates the effects of thermal broadening thus acting as a single broadener from multiple sources. To choose the proper projected rotation velocity, the spectral line must be selected when it is at its narrowest. This occurs when there is little to no radial velocity broadening or simply when $V_{rad} \approx 0$. There is minimal radial velocity broadening twice in each phase, at maximum and minimum radius. Since we are looking for the narrowest line, it makes sense to choose the observation closest to maximum radius where the projected rotation velocity is at its smallest. Because ζ_{ISO} affects mainly the wings of a spectral line and to a lesser extent, the core, a rough but reasonable value for ζ_{ISO} can be determined independent of $V_{rot} \sin i$. Then the projected rotation velocity can be increased until the core of the model spectral line is sufficiently broad to match the observed spectral line. After introducing the radial/tangential macroturbulence (ζ_{RT}) to improve the model's fit, the projected rotation velocity may be reduced slightly. This estimation for $V_{rot} \sin i$ is the value used for the remaining models for that particular star. The process described above is illustrated in Figure 2.

There is a basic assumption made in the previous paragraph that must now be proven before continuing. It was assumed that the projected rotation velocity remains constant over the entire phase of the pulsating star. This can be verified by determining the change in angular velocity between maximum and minimum radius. Using data from the Galactic Cepheid Database,[13] ζ Geminorum is found to have a mean radius $R_{ZG} = 64.9 R_{\odot} \approx 4.51 \times 10^7 km$. Using the data from Bersier et al.,[14] Kervella et al. (2001)[15] found ζ Geminorum's radius to oscillate by $+3.0 \times 10^6\, km$ and $-1.6 \times 10^6\, km$ from it's radius at zero phase. These values are later verified by our own calculations. The ratio and percent change can now be computed as follows:

$$\frac{R_{max}}{R_{min}} = \frac{4.81 \times 10^7}{4.35 \times 10^7} = 1.10 \tag{10}$$

$$\%\, change = \frac{R_{max} - R_{min}}{R_{ZG}} \times 100 = 10.\% \tag{11}$$

where R_{max} and R_{min} are the maximum and minimum radius. Using the equations for moment of inertia and conservation of angular momentum, it can be shown that the ratio of maximum to minimum angular velocity is:

$$\frac{\omega_{max}}{\omega_{min}} = \frac{R_{max}^2}{R_{min}^2} = (1.10)^2 = 1.22 \tag{12}$$

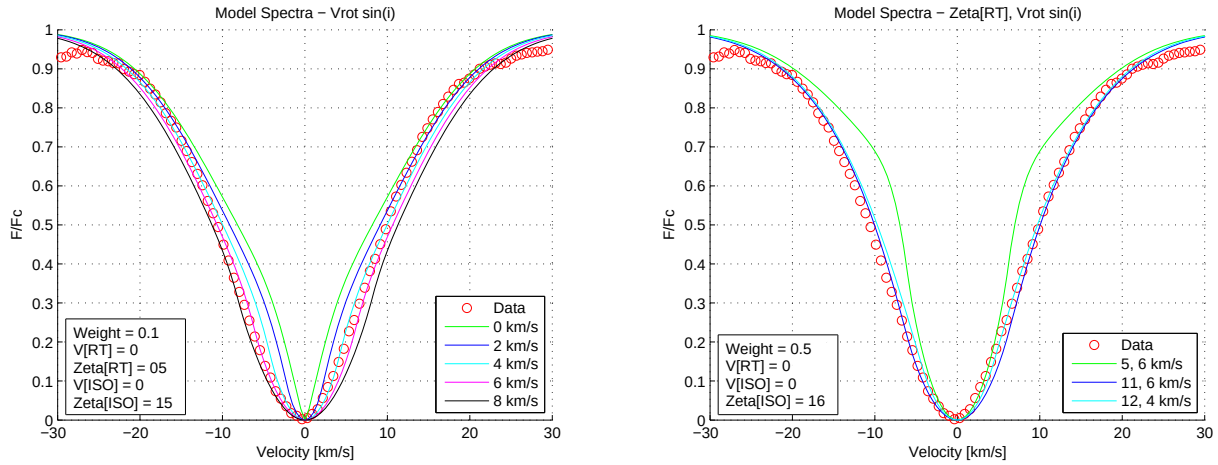

(a) (b)

Figure 2. The projected rotation velocity is a significant broadener in the core. Part (a) shows that in this case, the value used for $V_{rot} \sin i$ should not exceed 6 km/s. Once the radial/tangential macroturbulence (ζ_{RT}) is introduced to improve the fit in part (b), the projected rotation velocity must be further limited to no more than 4 km/s.

thus giving a percent change in angular velocity of approximately 20%. The largest $V_{rot} \sin i$ used is 5 km/s for δ Cephei thus resulting in a negligible (± 1 km/s) change in the projected rotation velocity over its period.

The limb darkening coefficient is used for modelling a uniform disk as a star by linearly darkening the disk as it approaches the edge or limb. This coefficient ranges between 0 and 1 where 0 signifies complete darkness and 1 signifies no darkening. Typical values usually fall between 0.64 and 0.75 for Cepheid variables thus we have chosen a value of 0.70 for all three stars. Nardetto et al.[3] use a value of 0.6721 for ζ Geminorum however when the limb darkening variable is modified by a few hundredths in DSKI4, there is no visible change between spectral lines as seen in part (a) of Figure 3. This suggests that fine tuning this factor with respect to phase or even from star to star will provide little to no benefit in the resulting pulsation velocity curves with our current precision.

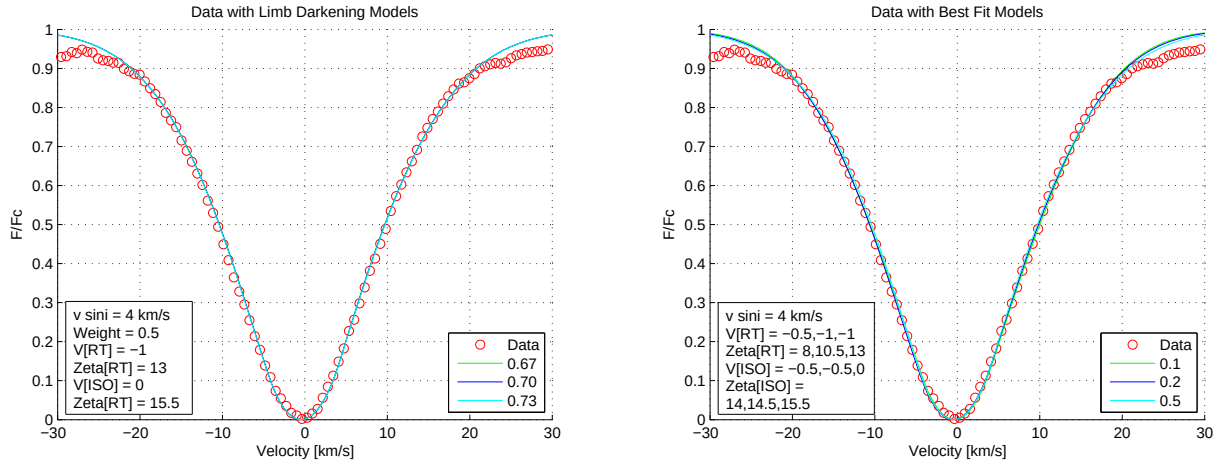

(a) (b)

Figure 3. (a) The limb darkening is set to values of 0.67, 0.70 and 0.73 in the DSKI4 modelling program but shows no visible differences in the resulting spectral line. (b) Using weights of 0.1, 0.2 and 0.5, an accurate fit of the observed spectral line can be obtained with each model.

How the contributions of the two radial velocity components are weighted is very important to the shape of the spectral line. The isotropic component is chosen to have a weight of 1.0 while the radial/tangential component is varied between 0.1 and 0.5. Different weights are tested and, when possible, a constant weight ratio is used over the entire phase for a particular star in an attempt to reduce the number of free parameters. Figure 4 shows the effects of different weight ratios at radial velocities of 0 and -20 km/s. The ζ ratio becomes more important as the difference between ζ_{RT} and ζ_{ISO} increases. Because of the soft restrictions on the necessary ratio, a fairly symmetric spectral line can usually be fitted with multiple models, each using a different weighting. An example of this is illustrated in part (b) of Figure 3. This may result in slightly different parameters, as seen in Table 2, however the resulting radial velocities are all well within the ± 0.7 error bar limit for V_{rad}.

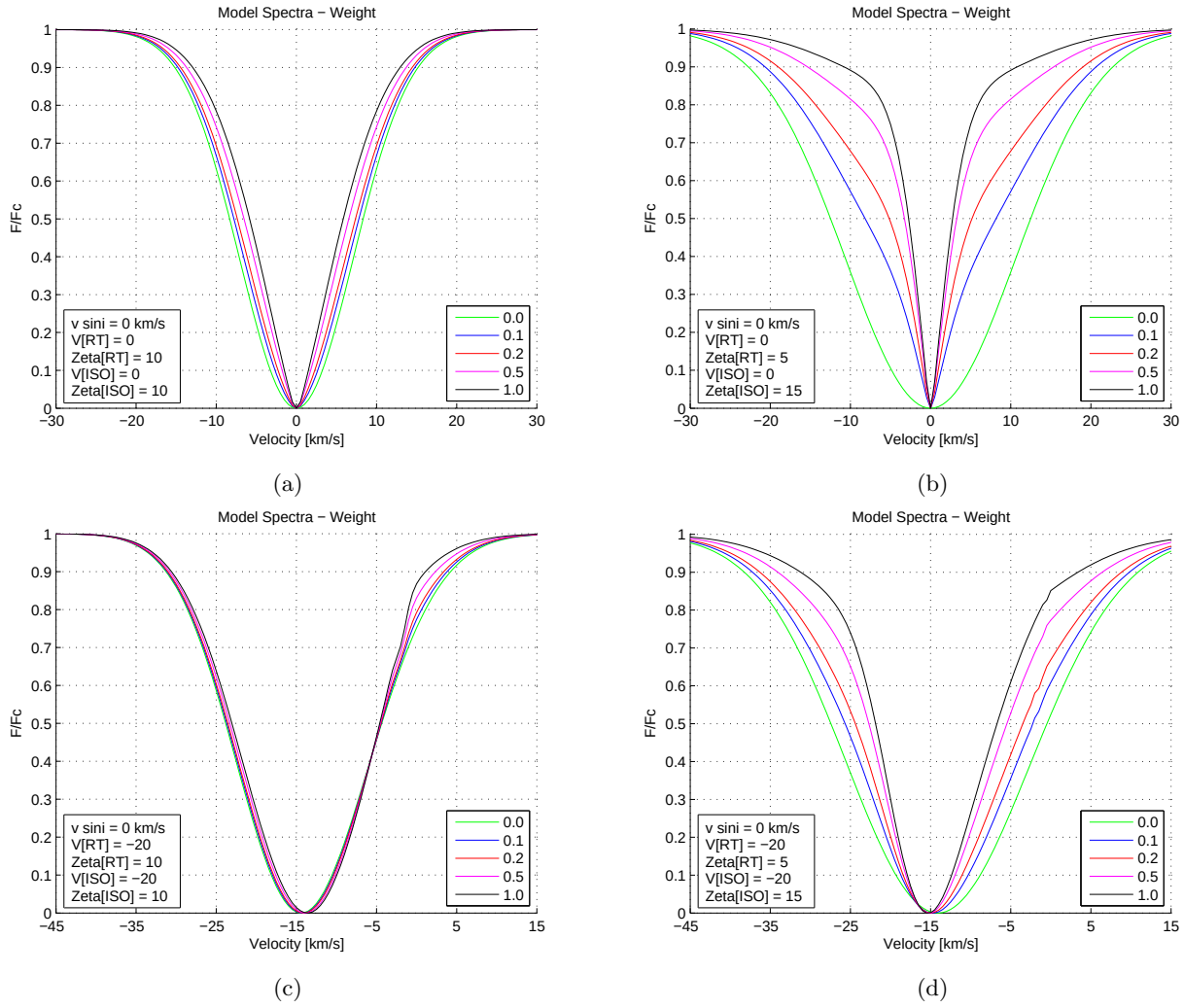

Figure 4. In parts (a) and (b), the differently weighted model lines experience no radial velocity shift while (c) and (d) see a shift of -20 km/s. Parts (a) and (c) show only a small dependence on the chosen ζ ratio while (b) and (d) are greatly affected in the shape of the spectral line. This dependence is magnified as the difference between ζ_{RT} and ζ_{ISO} increases.

More effects from systematically altering the variables in DSKI4 can be seen in Figure 5. The broadening of a model spectral line is illustrated in part (a) by systematically increasing $V_{rot} \sin i$ while in part (b) the spectral line is shifted by adjusting the radial velocity component. Part (c) uses the radial/tangential macroturbulence as a broadener and part (d) broadens the spectral line using the isotropic components. Neither ζ_{RT} or ζ_{ISO} was specifically incorporated in Nardetto et al.'s[3] toy model but were instead combined into an intrinsic width for the line (σ_C).

Model ζ ratio	0.1	0.2	0.5	
$V_{rot} \sin i$	4.0	4.0	4.0	$\pm$0.8
V_{RT}	-0.5	-1.0	-1.0	$\pm$0.5
ζ_{RT}	8.0	10.5	13.0	$\pm$0.5
V_{ISO}	-0.5	-0.5	0.0	$\pm$0.5
ζ_{ISO}	14.0	14.5	15.5	$\pm$0.5
V_{rad}	-0.5	-0.6	-0.3	$\pm$0.7

Table 2. Different ratios can be used to fit the same spectral line however the resulting radial velocities are relatively close.

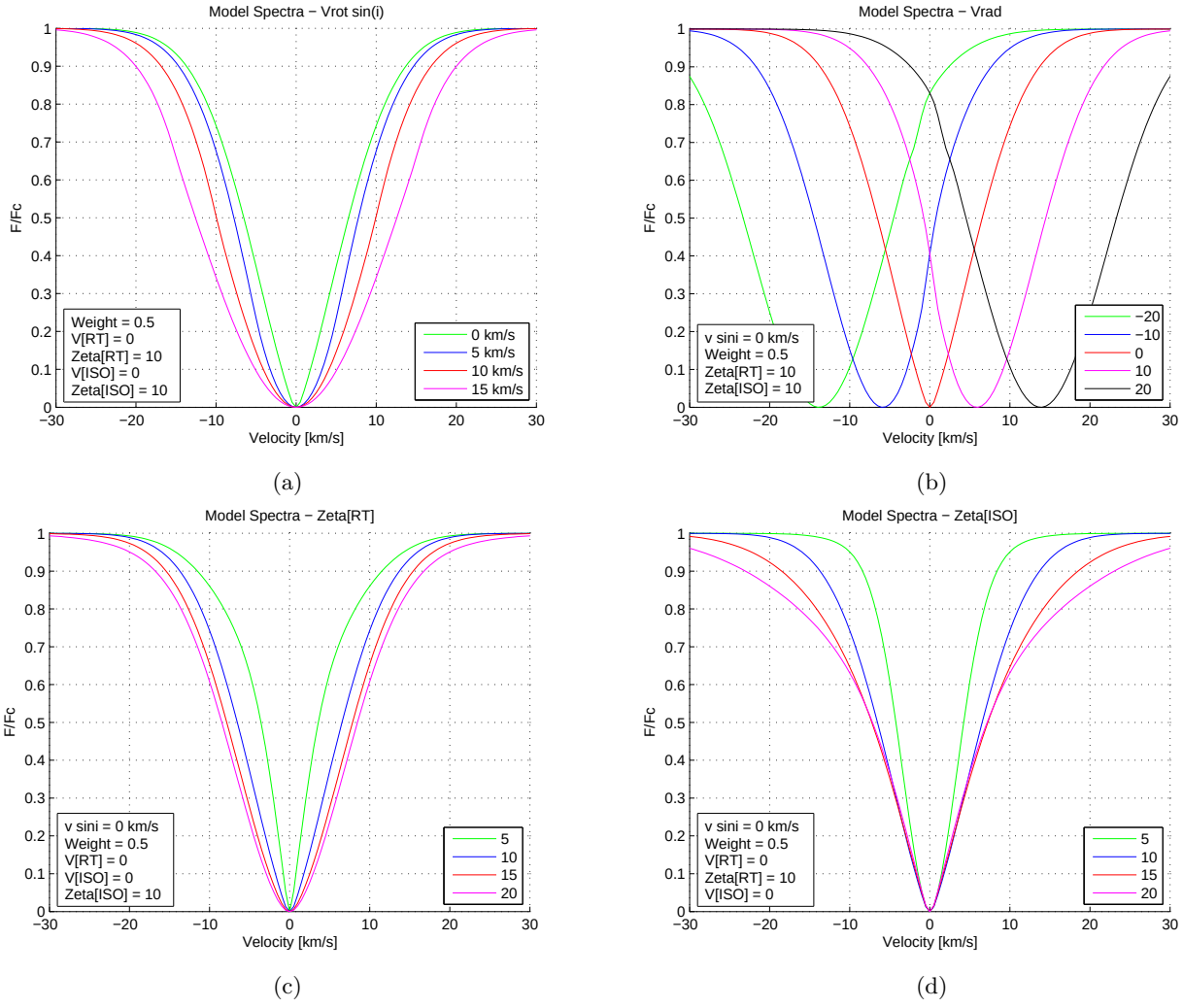

Figure 5. These spectral line models are produced by varying (a) the projected rotation velocity ($V_{rot} \sin i$), (b) the radial velocity (V_{rad}), (c) the radial/tangential macroturbulence (ζ_{RT}), and (d) the isotropic components (ζ_{ISO}).

3. ANALYSIS AND RESULTS

A total of 44 usable exposures have been obtained: 16 for δ Cephei, 11 for η Aquilae and 17 for ζ Geminorum. Adequate phase coverage for each of the Cepheid variables is necessary to produce accurate and reliable results. Figure 6 illustrates the phase coverage for δ Cephei, η Aquilae and ζ Geminorum.

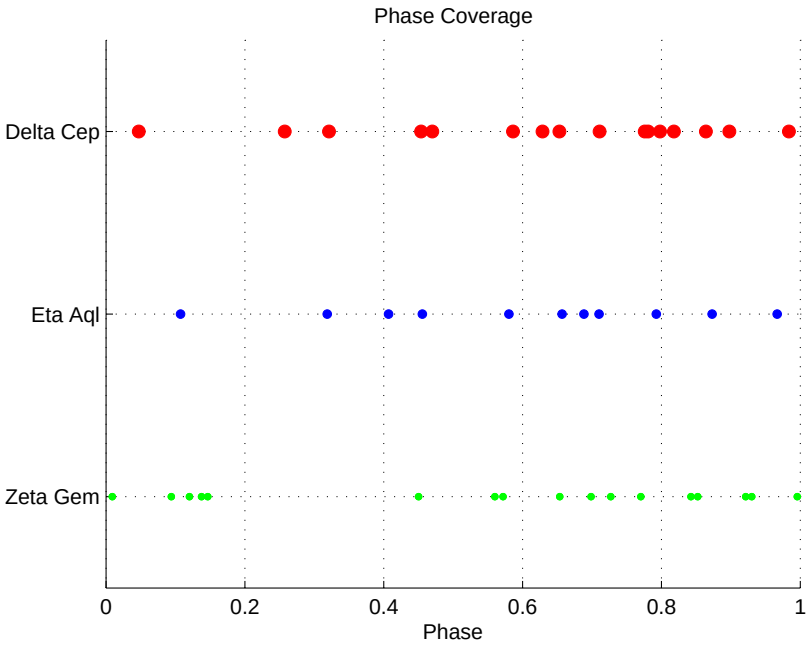

Figure 6. Phase coverage of δ Cephei, η Aquilae and ζ Geminorum. The diameter of the circles represents the phase span of a typical two hour exposure.

Each of the spectral lines is normalized by setting the continuum to a value of 1 and the peak to a value of 0. All of the remaining data points are then adjusted accordingly. This normalization allows the data to be easily compared to the models produced using DSKI4, which is described in the previous section, however some of the information is lost through this process. For example, an increase in temperature will increase the Fe II to Fe I ratio thus resulting in less Fe I and shallower Fe I lines. At the same time there will be more Fe II hence their spectral lines will become deeper. Fortunately, this change in temperature does not affect the spectral line's shape thus leaving the pulsation velocity curve unaffected. In order to reduce the amount of noise in the exposures, several of the chosen spectral lines can be added together through averaging. The four Fe I lines (6231, 6233, 6253 and 6265 Å) are similar enough to be averaged together, once normalized. The Fe II lines (6238 and 6248 Å) are too broad as compared to the Fe I lines and as such, are not used for averaging.

Prior to the averaging technique, the spectral lines are converted from a wavelength to a velocity span using equation (4). The values of the reference wavelengths are: 6230.74, 6232.65, 6252.57 and 6265.16 Å for the four lines while the reference velocity is the systemic radial velocity, v_γ, for each Cepheid. The velocities of the spectral lines are now in the reference frame of their respective stars which is necessary when correctly fitting with a model. The evolution of the averaged, normalized spectral line for each Cepheid (δ Cephei, η Aquilae and ζ Geminorum) is displayed in Figure 7. The evident shifts in the spectral lines are a result of the changing radial velocities, as are the asymmetries, both of which will be discussed in further detail.

The best fitting model is chosen by trial and error using the knowledge of how each variable affects a spectral line at a given phase. Once a suitable model has been found, its parameters can describe the star's physical characteristics at that point in its phase. However, fitting all of the observed spectral lines with individual models is very difficult and time consuming. Despite having a large number of free parameters to work with, sometimes the model cannot be fitted perfectly to the observed data. Some examples of this can be seen for η Aquilae in part (a) of Figure 8, where some parts of the model will not coincide with the observed data. In part (b), the models for ζ Geminorum more accurately reflect the observed line with some exceptions near the continuum as a result of blending. These two examples serve to illustrate the complex nature of fitting by hand and the potential need for a more precise and robust method.

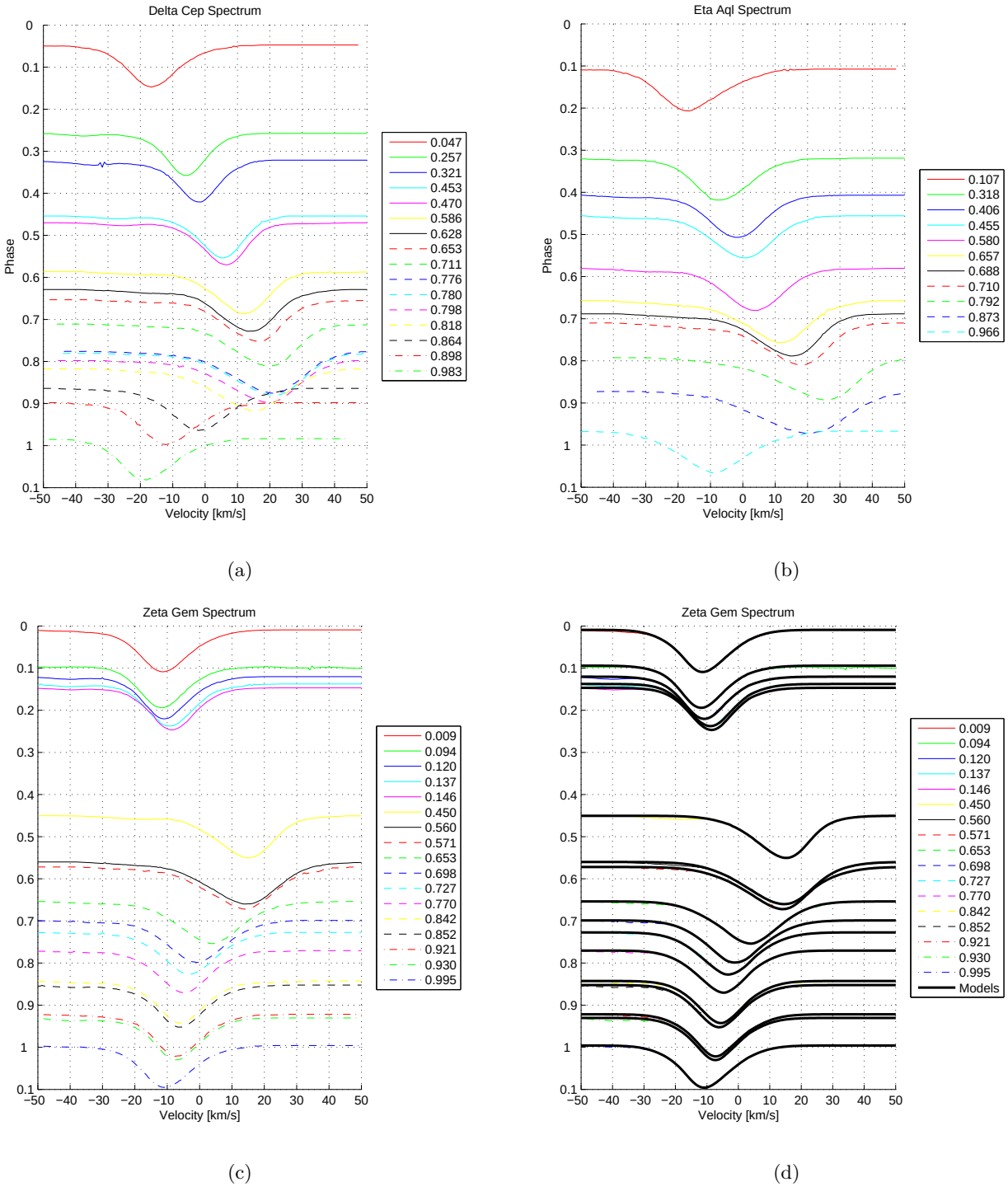

Figure 7. Evolution of (a) δ Cephei, (b) η Aquilae and (c) ζ Geminorum's normalized, averaged spectral lines in velocity units. The ordinate represents the phase at each exposure's continuum. Part (d) overlays ζ Geminorum's observed spectrum with the models produced by DSKI4.

At certain stages in a Cepheid's phase, namely maximum and minimum radial velocity, the spectral lines show significant asymmetry. At its minimum radial velocity, the bisector is distinctly "C" shaped while at maximum radial velocity the bisector's shape is inverted, looking more like a ")" shape. This effect is illustrated in Figure 8 where the curvature of the bisectors has been magnified by a factor of two. The observed asymmetry is a result of the star's differentially expanding and contracting atmosphere. This implies that there will be a smaller radial velocity at the formation depth of a spectral line's wings ($\log \tau \approx -1$) than at higher layers near the formation depth of the core ($\log \tau \approx -3$). Because the wings of the spectral line are significantly less shifted than the core, the result is an asymmetric spectral line. Albrow at al.[12] provide an example model to illustrate this point. At a phase of 0.57, the velocity at the core's depth of formation is $\sim 10\,km/s$ while only $\sim 3\,km/s$ at the formation depth of the wings. The spectral line's "blue" wing is formed in a nearly static atmosphere with a significant flux contribution while the "red" wing makes no contribution due to the overlapping, redshifted core. The observed core ($\sim 5\,km/s$ in this example) is a combination of the two major contributors.

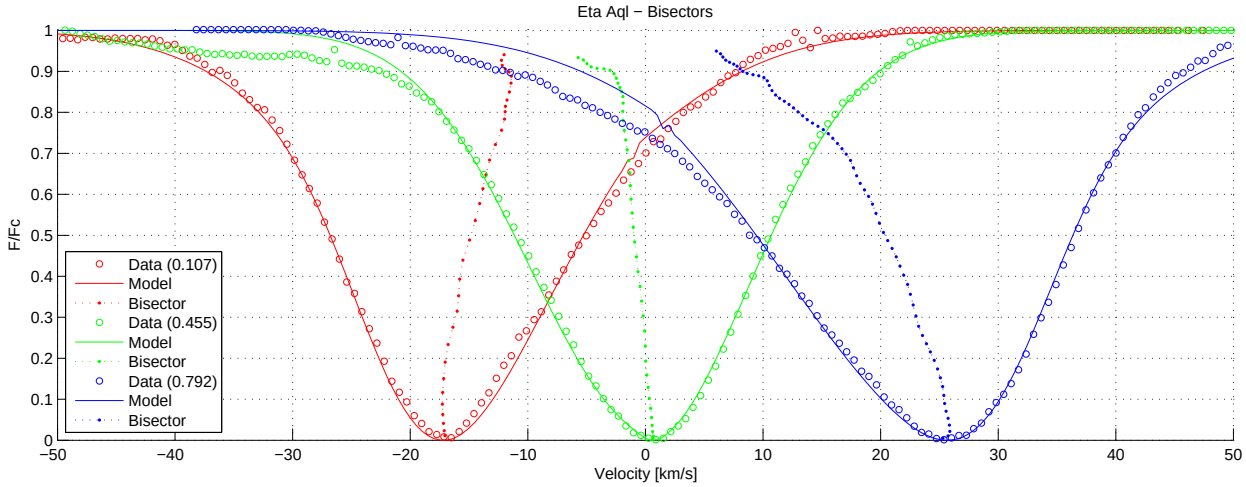

(a)

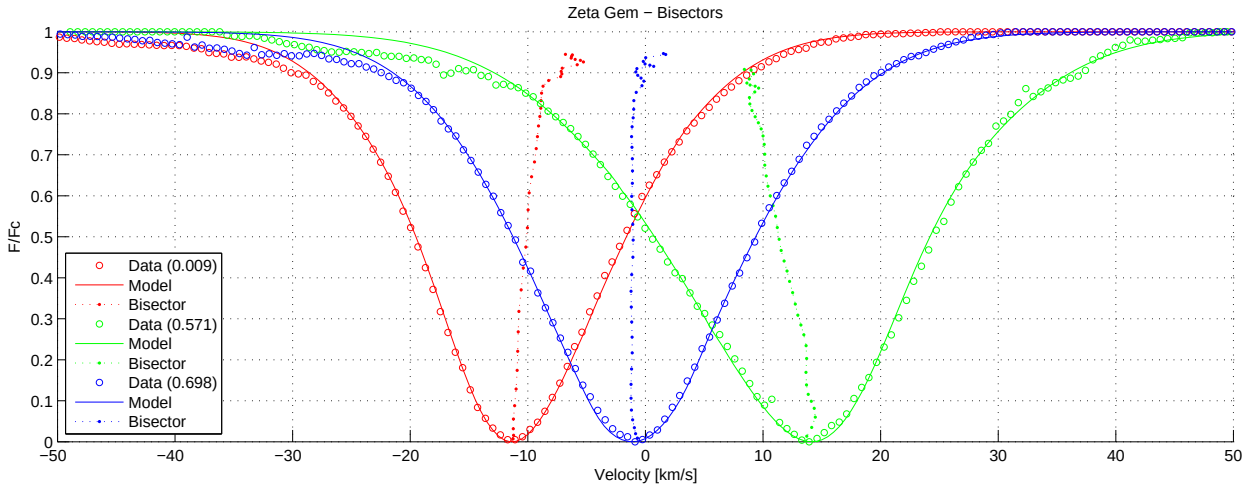

(b)

Figure 8. The sample models for (a) η Aquilae do not fit as well as the sample models for (b) ζ Geminorum. The bisectors for both stars are magnified by a factor of two to clearly show their changes in curvatures with phase. Noise in the continuum can impact the bisector above $F/F_C = 0.9$ thus should not be considered reliable above this point.

Once the pulsation velocities are determined, the resulting points are plotted as a function of phase and

Star	Data Set	v_γ $[km/s]$	p	Area	ΔR_{avg} $[10^6\ km]$
δ Cephei	Stevenson	-17.8	-	-0.21	3.54
	Barnes (2005)	-17.8	1.36	1.28†	3.43
	Bersier (1994)	-17.8	1.36	-0.83†	3.42
η Aquilae	Stevenson	-15.8	-	0.05	4.59
	Barnes (2005)	-15.8	1.36	1.48†	4.57
	Bersier (2002)	-15.8	1.36	1.06†	4.43
ζ Geminorum	Stevenson	5.8	-	-0.09†	4.75
	Nardetto (2006)	5.8	1.40	1.81	4.51
	Bersier (1994)	5.8	1.36	0.01†	4.75
		± 0.5			± 0.10

Table 3. Values used for the systemic radial velocity, the projection factor (if necessary), and the resulting area for each of the pulsation velocity curves. The amplitude of the radius variation, between R_{max} and R_{min}, is computed using our technique for each of the pulsation velocity curves.

a cubic spline is used to fit the data with a curve then extrapolate a pulsation velocity between observations. Integrating this velocity curve should result in a net area of zero, otherwise the star would not return to the same state upon each cycle through its period. If the value is not zero then the systemic radial velocity (v_γ) can be adjusted accordingly and the models must be reproduced and refitted to the data thus resulting in a new pulsation velocity curve and a new area. This process is repeated until an area of zero is reached. The final pulsation velocity curves are illustrated in Figure 9 along with the extrapolated results from Barnes et al.,[16] Bersier et al.[14] and Nardetto et al.[3] using the paramters listed in Table 3. For ζ Geminorum, the large gap in phase coverage between 0.2 and 0.4 is overcome by using 2 data points from Bersier et al.[14] Table 3 also lists some numerical results from the final iterations.

In Figure 9, all of the ephemeris have been adjusted to the values specified in Table 1 while the periods have been preserved as the values used in their respective papers. By choosing the same zero point, this removes any horizontal shifts in the data due to less precise maximum intensity measurements. Some of these Cepheids' periods, specially ζ Geminorum, change quite rapidly thus making it unsuitable to use the same period for measurements that were taken several years apart.[4] The small differences between the authors' pulsation velocity curves for a particular Cepheid can be attributed to errors in the different methods used for determining the radial velocities. For example, our results are limited by our ability to model the observed spectral lines. Barnes at al. use a standard star instead of a telluric lamp thus resulting in various sources of error which may include an error in the adopted radial velocity of the standard star, uncertainty due to mispositioning of either star in the spectrograph slit, and uncertainty due to potential differences in the velocity scales of Cepheids and the mainsequence standards.[16]

Although an absolute radius is unobtainable using spectroscopy alone, the amplitude of the radius variation is achievable and very useful when applied to the Baade-Wesselink method described in Section 1. The fitted pulsation velocity curves in Figure 9 use an ordinate spacing of 0.01 periods. Using each Cepheid's period, the spacing is converted into a time interval (in seconds) and multiplied by its current pulsation velocity. These results are then added up between maximum and minimum radius, or between roots in the pulsation velocity curve, to determine the amplitude of radius variation ($R_{max} - R_{min}$) for each Cepheid. To increase the precision by removing the effects of a nonzero area, both $R_{max} - R_{min}$ and $|R_{min} - R_{max}|$ are calculated using the positive and negative portions, respectively, of the pulsation velocity curve then averaged to arrive at a final value, ΔR_{avg}. ζ Geminorum's radial amplitude is found to be $(4.75 \pm 0.10) \times 10^6\ km$ using $v_\gamma = 5.8\ km/s$. In comparison, Kervella et al. (2001)[15] computed an amplitude of $4.64 \times 10^6\ km$ using Bersier et al.'s[14] data from 1994 with $v_\gamma = 5.83\ km/s$ and $p = 1.36$. Using our method of calculation with Bersier et al.'s data and nearly identical parameters listed in Table 3, we still compute an amplitude of $(4.75 \pm 0.10) \times 10^6\ km$. Differences in these

†Some of the closely spaced data points were removed to improve the cubic spline's overall form

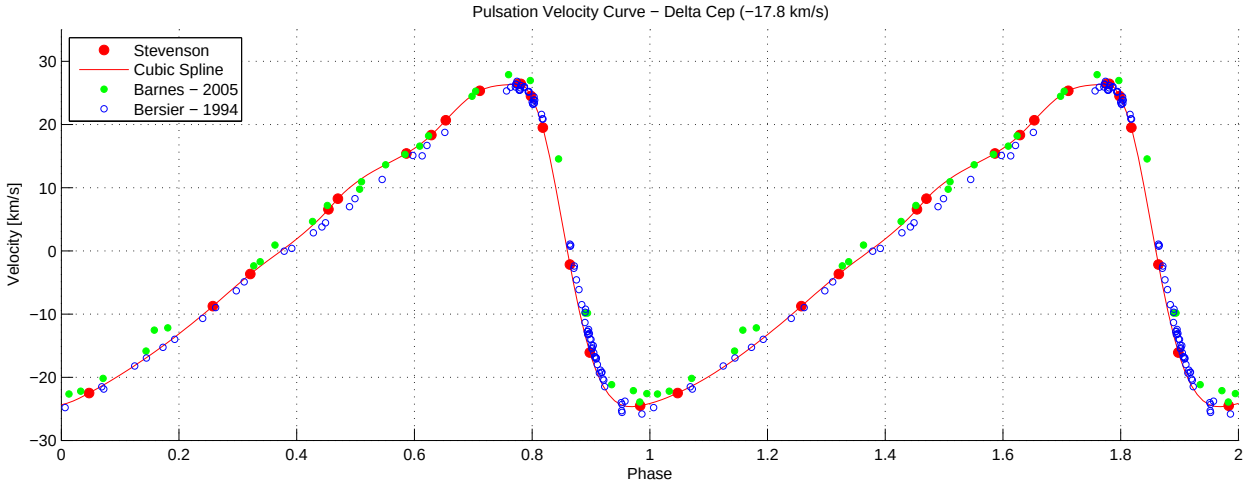

(a)

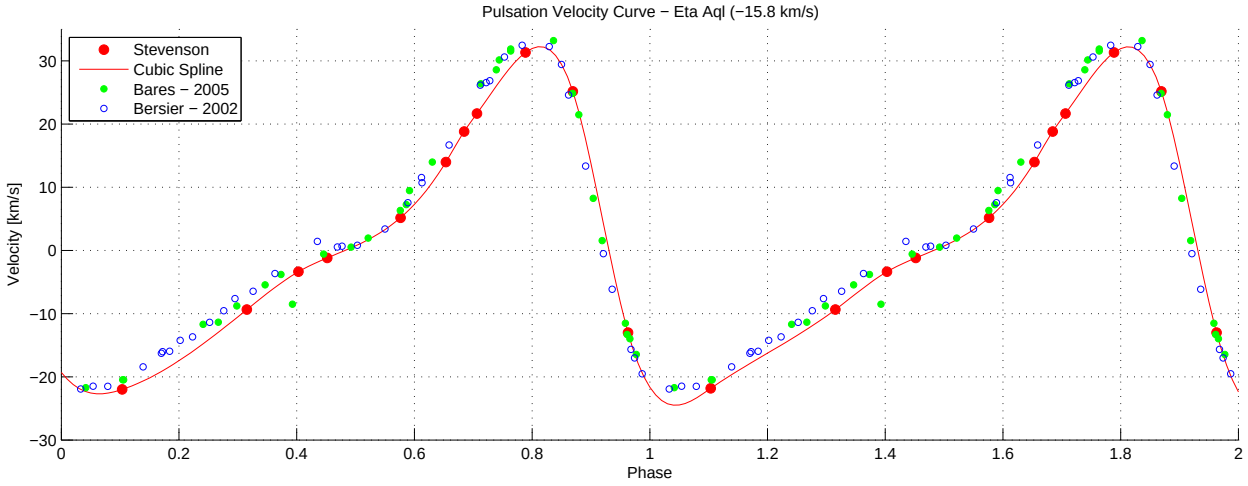

(b)

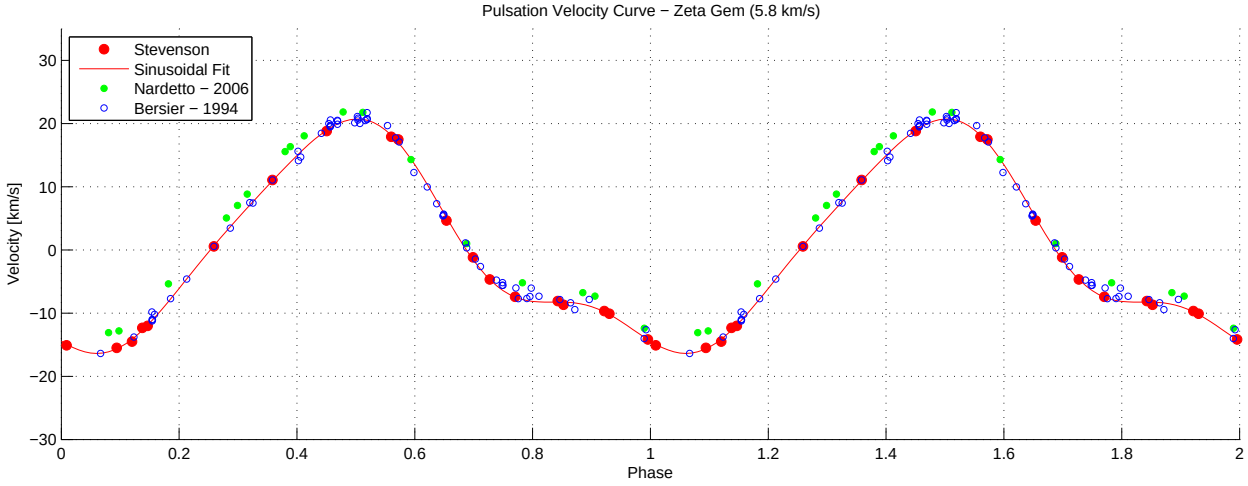

(c)

Figure 9. Pulsation velocity curves for (a) δ Cephei, (b) η Aquilae and (c) ζ Geminorum with systemic radial velocities of -17.8, -15.8 and 5.8 km/s.

Star	Stevenson [10^6 km]	Kervella (2001)[15] [10^6 km]	Kervella (2004)[1] [10^6 km]	Moskalik[17] [10^6 km]
δ Cephei	3.54	-	-	3.40
η Aquilae	4.59	-	4.38	4.45
ζ Geminorum	4.75	4.64	4.90	4.68
	$\pm$0.10	-	$\pm$0.8	-

Table 4. A comparison between our amplitude of radius variation results and other authors

results are likely due to Kervella et al.'s choice in period for ζ Geminorum. They use $\Pi = 10.150079$ instead of 10.149955 days as calculated by Bersier et al. using Equation 9. For all of the numerical calculations of ΔR_{avg} refer to Table 3 and for more comparisons between other authors' results see Table 4. The results from Kervella at al. (2004)[1] were computed using Equation 3 while Moskalik & Gorynya's[17] values are predicted results based on calculations.

Integrating a pulsation velocity curve that has no effective area will give the change in radius as a function of phase. The Cepheids' radial displacement curves are plotted in Figure 10, where the variations are relative to each star's radius at maximum luminosity. By inspecting ζ Geminorum's curve, it can be easily verified that the amplitude of the radius variation, $\Delta R_{avg} = 4.75 \times 10^6\ km$, as calculated above. As mentioned in Section 2, Kervella et al.[15] found ζ Geminorum's radius to oscillate by $+3.0 \times 10^6\ km$ and $-1.6 \times 10^6\ km$ from its zero point. Our results indicate a much more symmetric oscillation of $+2.53 \times 10^6\ km$ and $-2.22 \times 10^6\ km$ about zero but this difference is mostly a result of the chosen ephemeris for zero phase.

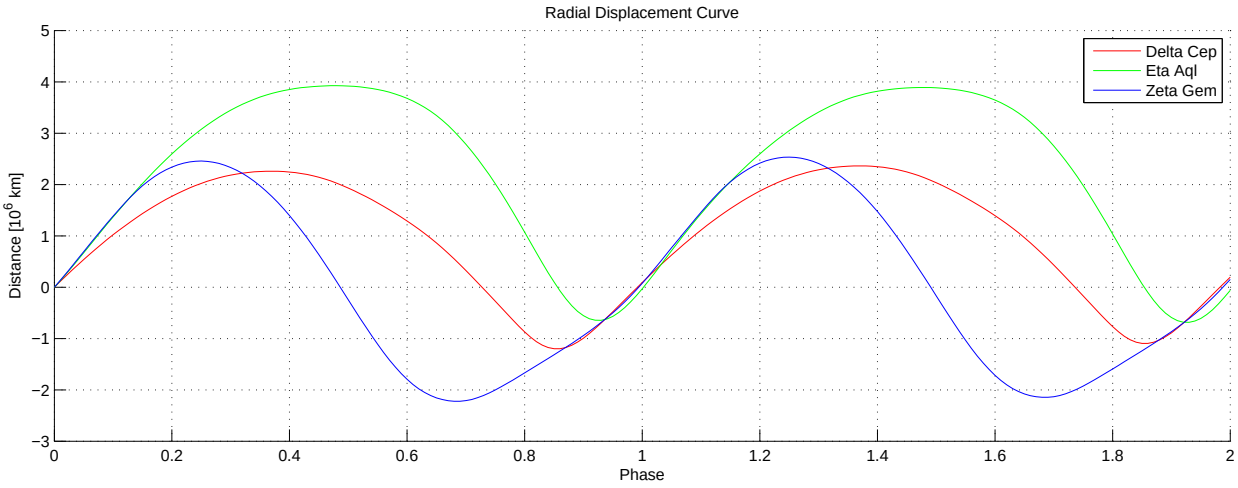

Figure 10. Integrated radial velocity curves for δ Cephei, η Aquilae and ζ Geminorum with respect to their radii at maximum luminosity. The curves' amplitudes agree with the above numerical calculations of ΔR_{avg}.

4. CONCLUSIONS

Pulsation velocity curves have been developed for three Cepheid variables: δ Cephei, η Aquilae and ζ Geminorum, using models created by a custom software package. No hydrodynamics are used nor are they required to create acceptable models that accurately fit the observed data. The resulting physical parameters are thus a product of geometric arguments which completely bypass the complicated physics that occur within the star. The pulsation velocity curves are compared against results from Barnes et al., Bersier et al. and Nardetto et al. with acceptable agreement. An important difference, however, is that our results have been achieved without the use

of a projection factor, p. All of the major contributors of line broadeners and sources of asymmetry have been taken into account. As such, our unaltered pulsation velocity curves are consistent with previously published results and have only slightly larger error bars.

Using the pulsation velocity curves created by our unique modelling method, the amplitude of radius variation ($\Delta R_{avg} = R_{max} - R_{min}$) has been determined for each of the Cepheids. The amplitudes for δ Cephei, η Aquilae and ζ Geminorum are $3.54 \times 10^6\ km$, $4.59 \times 10^6\ km$ and $4.75 \times 10^6\ km$, respectively. These results coincide with those from Barnes and Bersier, using the parameters in Table 3, with differences of $< 3.5\%$ or within $0.16 \times 10^6\ km$. The difference in results from the data provided by Nardetto are slightly larger at 5%. They used a projection factor of 1.40 and line centroid based methods for calculating pulsation velocities, thus resulting in an amplitude of $4.51 \times 10^6\ km$ for ζ Geminorum. The error in our results is $\pm 0.10 \times 10^6\ km$.

At this point, more observations and better phase coverage are needed to improve the accuracy and precision of our results. The current errors can be decreased by averaging results within a given phase interval or by devising a more robust method for modelling the observed spectral lines.

REFERENCES

1. P. Kervella, N. Nardetto, D. Bersier, D. Mourard, and V. Coudé du Foresto, "Cepheid distances from infrared long-baseline interferometry. I. VINCI/VLTI observations of seven Galactic Cepheids," *Astronomy and Astrophysics* **416**, pp. 941–953, 2004.
2. J. P. Cox, *Pulsating Stars*, Joint Institute for Laboratory Astrophysics, University of Colorado and National Bureau of Standards and Department of Physics and Astrophysics, University of Colorado, Boulder, Colorado 80302, USA, 1974.
3. N. Nardetto, D. Mourard, P. Kervella, P. Mathias, A. Mrand, and D. Bersier, "High resolution spectroscopy for Cepheids distance determination I. Line asymmetry," *Astronomy and Astrophysics* **453**, pp. 309–319, 2006.
4. L. Szabados, "Northern cepheids: Period update and duplicity effects," *Comm. Konkoly Observatory* **96**, 1991.
5. *The Astronomical Almanac for the Year 2006*, TSO, 2004.
6. Kholopov+, *Combined General Catalogue of Variable Stars (Vol. I-III)*, 1998.
7. D. F. Gray, "Measurement of line profiles," *IN: Instrumentation and research programmes for small telescopes; Proceedings of the IAU Symposium* , pp. 401–411, 1986.
8. D. F. Gray, C. Tycner, and K. Brown, "Spectral-line profiles in daytime skylight," *PASP* **112**, pp. 328–334, 2000.
9. K. Brown, private communication, 2006.
10. D. F. Gray, *Lectures on Spectral-Line Analysis: F, G, and K Stars*, The Publisher: Arva, Ontario, 1988.
11. D. F. Gray and K. I. T. Brown, "Precise spectroscopic radial velocity measurements using telluric lines," *PASP* **118**, pp. 399–404, 2006.
12. M. D. Albrow and P. L. Cottrell, "Contribution functions and the depths of formation of spectral lines in cepheids," *Royal Astronomical Society* **278**, pp. 337–344, 1996.
13. J. D. Fernie, B. Beattie, and N. R. E. nd S Seager, "http://www.astro.utoronto.ca/ddo/research/cepheids/," *IBVS No. 4148* , 1995.
14. D. Bersier, G. Burki, M. Mayor, and A. Duquennoy, "Fundamental parameters of Cepheids. II. Radial velocity data," *Astronomy and Astrophysics* **108**, pp. 25–39, 1994.
15. P. Kervella, V. Coudé du Foresto, G. Perrin, M. Scholler, W. A. Traub, and M. G. Lacasse, "The angular diameter and distance of the Cepheid ζ Geminorum," *Astronomy and Astrophysics* **367**, pp. 876–883, 2001.
16. T. G. Barnes, E. J. Jeffery, T. J. Montemayor, and I. Skillen, "Radial velocities of galactic cepheids," *The Astrophysical Journal Supplement Series* **156**, pp. 227–235, 2005.
17. P. Moskalik and N. A. Gorynya, "Mean Angular Diameters and Angular Diameter Amplitudes of Bright Cepheids," *Acta Astronomica* **55**, pp. 247–260, 2005.

Phase	JD	S/N[‡]	Lines[§]	ζ Ratio[¶]	V_{RT} $[km/s]$	ζ_{RT} $[km/s]$	V_{ISO} $[km/s]$	ζ_{ISO} $[km/s]$	$V_{rot}\sin i$ $[km/s]$	V_{puls} $[km/s]$	Filename	Observer[‖]
0.0473	13902.684	363	4	0.2	-20.0	4.0	-23.0	10.5	5.0	-22.50	JN1506v.077	KBS
0.2576	13930.644	326	4	0.2	-7.5	5.5	-9.0	9.5	5.0	-8.75	JL1306v.095	KBS
0.3212	13925.619	155	4	0.2	-2.0	5.0	-4.0	10.5	5.0	-3.67	JL0806v.093	KBS
0.4539	13845.836	300	4	0.3	8.5	6.0	6.0	11.0	5.0	6.58	AP1906v.066	KBS
0.4701	13679.566	302	4	0.2	9.5	5.0	8.0	10.5	5.0	8.25	NO0405v.002	KBS
0.5864	13878.745	182	4	0.2	17.5	5.0	15.0	11.5	5.0	15.42	MY2206v.073	KBS
0.6289	13932.636	167	4	0.2	20.0	6.0	18.0	12.0	5.0	18.33	JL1506v.099	KBS
0.6532	13916.668	139	4	0.2	21.5	5.0	20.5	12.5	5.0	20.67	JN2906v.082	KBS
0.7111	13841.850	143	4	0.2	27.0	5.0	25.0	12.5	5.0	25.33	AP1506v.055	KBS
0.7761	13922.694	225	4	0.2	28.5	6.0	26.0	14.5	5.0	26.42	JL0506v.089	KBS
0.7808	13686.600	253	4	0.2	28.5	6.0	26.0	14.5	5.0	26.42	NO1105v.007	KBS
0.7980	13686.692	312	4	0.2	27.0	6.0	24.0	14.5	5.0	24.50	NO1105v.008	KBS
0.8181	13933.652	217	4	0.2	22.0	7.0	19.0	15.5	5.0	19.50	JL1606v.104	KBS
0.8641	13917.800	281	4	0.2	-3.0	9.5	-2.0	15.0	5.0	-2.17	JN3006v.086	KBS
0.8980	13842.853	191	4	0.2	-16.5	5.0	-16.0	13.0	5.0	-16.08	AP1606v.060	KBS
0.9837	13923.808	275	4	0.2	-22.0	4.0	-25.0	10.0	5.0	-24.50	JL0606q.217	DFG
					± 0.5	± 0.5	± 0.5	± 0.5	± 1.0	± 0.71		

Table 5. Observational data for δ Cephei

[‡]Signal to noise ratio for the given exposure

[§]Number of spectral lines used when averaging

[¶]Weighted ratio of ζ_{RT} and ζ_{ISO}

[‖]Observations made by Kevin B. Stevenson (KBS), Dr. David F. Gray (DFG) and Kevin Brown (KB)

Phase	JD	S/N‡	Lines§	ζ Ratio¶	V_{RT} $[km/s]$	ζ_{RT} $[km/s]$	V_{ISO} $[km/s]$	ζ_{ISO} $[km/s]$	$V_{rot}\sin i$ $[km/s]$	V_{puls} $[km/s]$	Filename	Observer‖
0.1075	13933.744	283	4	0.5	-24.0	7.0	-21.0	16.5	0.0	-22.00	JL1606v.105	KBS
0.3188	13662.547	332	4	0.1	-13.0	7.0	-9.0	13.0	0.0	-9.36	OC1805q.183	DFG
0.4070	13892.834	346	4	0.1	-2.0	13.0	-3.5	12.5	0.0	-3.36	JN0506j.932	KB
0.4557	13878.830	261	4	0.1	7.0	13.0	-2.0	13.5	0.0	-1.18	MY2206v.074	KBS
0.5804	13922.785	211	4	0.1	12.0	13.0	4.5	13.0	0.0	5.18	JL0506v.090	KBS
0.6571	13686.505	178	4	0.2	19.0	6.0	13.0	16.0	0.0	14.00	NO1105v.006	KBS
0.6885	13930.738	302	4	0.2	23.0	5.0	18.0	13.5	0.0	18.83	JL1306v.096	KBS
0.7102	13923.717	246	3	0.5	26.0	7.0	19.5	16.0	0.0	21.67	JL0606q.216	DFG
0.7928	13902.779	251	4	0.5	34.0	7.0	30.0	18.0	0.0	31.33	JN1506v.078	KBS
0.8731	13917.709	214	4	0.2	31.0	9.0	24.0	19.0	0.0	25.17	JN3006v.085	KBS
0.9669	13932.735	298	4	0.1	-13.0	6.0	-13.0	16.5	0.0	-13.00	JL1506v.100	KBS
					± 0.5	± 0.5	± 0.5	± 0.5	$+0.5$	± 0.71		

Table 6. Observational data for η Aquilae

Phase	JD	S/N‡	Lines§	ζ Ratio¶	V_{RT} $[km/s]$	ζ_{RT} $[km/s]$	V_{ISO} $[km/s]$	ζ_{ISO} $[km/s]$	$V_{rot}\sin i$ $[km/s]$	V_{puls} $[km/s]$	Filename	Observer‖
0.0090	13834.597	272	4	0.2	-15.5	5.0	-15.0	12.0	4.0	-15.08	AP0806v.042	KBS
0.0941	13845.609	302	4	0.5	-16.5	6.0	-15.0	12.5	4.0	-15.50	AP1906v.062	KBS
0.1202	13825.577	273	3	0.5	-15.5	6.5	-14.0	12.5	4.0	-14.50	MR3006v.036	KBS
0.1376	13815.604	210	3	0.5	-14.0	8.0	-11.5	12.0	4.0	-12.33	MR2006v.029	KBS
0.1466	13815.696	143	4	0.5	-13.0	7.5	-11.5	12.0	4.0	-12.00	MR2006v.030	KBS
0.4504	13686.842	258	4	0.5	21.5	6.5	17.5	14.0	4.0	18.83	NO1105v.010	KBS
0.5601	13799.594	261	4	0.2	22.5	7.0	17.0	16.0	4.0	17.92	MR0406j.879	KB
0.5720	13860.609	160	4	0.2	20.0	6.0	17.0	16.5	4.0	17.50	MY0406Q.202	DFG
0.6538	13810.694	311	4	0.2	8.0	11.0	4.0	15.5	4.0	4.67	MR1506v.021	KBS
0.6988	13841.598	204	4	0.5	-2.5	14.0	-0.5	15.0	4.0	-1.17	AP1506v.051	KBS
0.7272	13821.589	305	4	0.5	-6.0	13.0	-4.0	14.5	4.0	-4.67	MR2606j.894	KB
0.7704	13679.940	237	4	0.2	-7.0	8.5	-7.5	13.0	4.0	-7.42	NO0405v.005	KBS
0.8426	13812.610	257	3	0.2	-8.5	7.0	-8.0	12.0	4.0	-8.08	MR1706v.024	KBS
0.8523	13812.709	234	4	0.2	-9.5	7.0	-8.5	12.0	4.0	-8.67	MR1706v.025	KBS
0.9216	13762.667	257	4	0.2	-10.5	5.5	-9.5	12.5	4.0	-9.67	JA2606Q.192	DFG
0.9303	13762.756	249	4	0.2	-10.5	5.5	-10.0	12.0	4.0	-10.08	JA2606Q.193	DFG
0.9958	13844.612	342	4	0.2	-15.0	5.0	-14.0	12.5	4.0	-14.17	AP1806q.196	DFG
					± 0.5	± 0.5	± 0.5	± 0.5	± 0.8	± 0.71		

Table 7. Observational data for ζ Geminorum